

Chapter 1

Introduction

Fluid management in compensated gravity environment is an important aspect of current and future space missions. The knowledge of liquid behavior in microgravity is essential for the development of space applications such as fluid management devices, life support systems or heat pipes. The simplicity, reliability and efficiency are here the key factors. Capillary techniques with free liquid surfaces are therefore an important element of fluid management in space. Having no moving parts, they provide a very reliable method of liquid control. Such devices are commonly two-phase systems, where free liquid surfaces are exposed to the gaseous phase. Hydrostatic pressure is negligible under microgravity conditions, and the influence of other forces dominates the behavior of the gas-liquid interfaces.

Typical applications are propellant management devices (PMDs) employed in satellite surface tension tanks (Figure 1.1). Propellant tanks are commonly spherical structures made of titan [65], where the ullage volume of withdrawn propellant is replaced by gas.

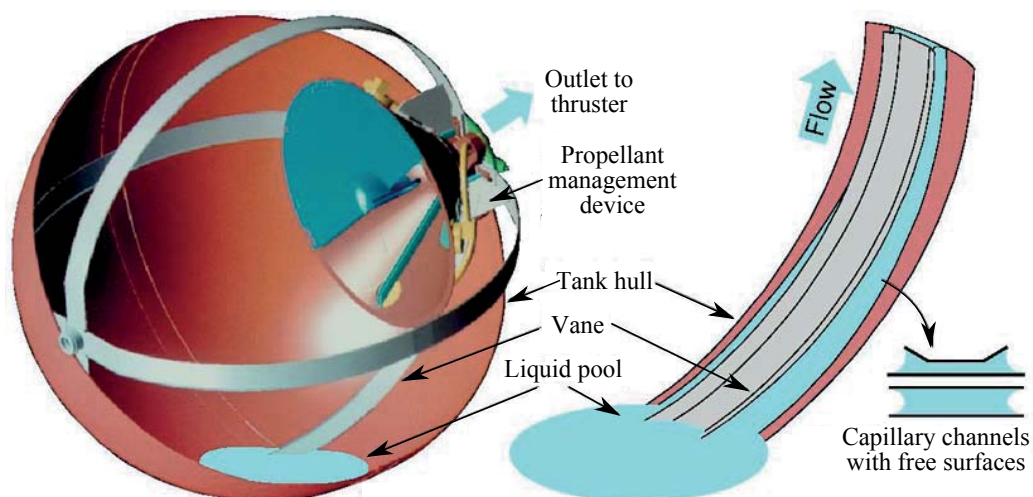


Figure 1.1: Satellite surface tension tank with a PMD consisting of capillary vanes.

The remaining propellant forms a bulk which is free to move within the tank depending on the spacecraft manoeuvre. A continuous, bubble-free flow between the propellant bulk and an outlet to the thruster is required during the entire manoeuvre phase. To achieve this, the tanks are equipped with propellant management devices. Because of chemical properties (aggressiveness) of the propellants, the choice of materials that can be used for the inner structure of the tank is very limited. The simplest PMD (Figure 1.1) consists of several metal plates aligned along the tank's inner walls [10, 43]. The plates are mounted close to the tank wall, forming vanes. The gap between the plates and the wall serves as a passage through which the propellant is transported towards the “funnel” part at the outlet of the PMD. From here, the propellant is driven directly to the thruster. Surface tension effects (capillary pressure) dominate the flow in the said passages where, depending on the design of the vanes, one or two free liquid surfaces are formed. The flow is driven by the pressure difference between the “funnel” and the propellant bulk. The curvature of the free surface adjusts to the changing pressure gradient between the liquid and the surrounding gas. Consequently, the free surfaces act as dampers compensating the pressure disturbances in case of the irregular propellant withdrawal. The propellant remains within the vanes due to adhesion and cohesion and the resulting capillary pressure. The stability of the flow in said vanes is essential for the mission performance. Under certain flow conditions, the free surface loses its stability and the flow becomes unstable. As a consequence, the surrounding gas is ingested into the flow path. Two-phase flow caused by the gas ingestion could be unfavorable for the application (lower efficiency or even damage of the thruster).

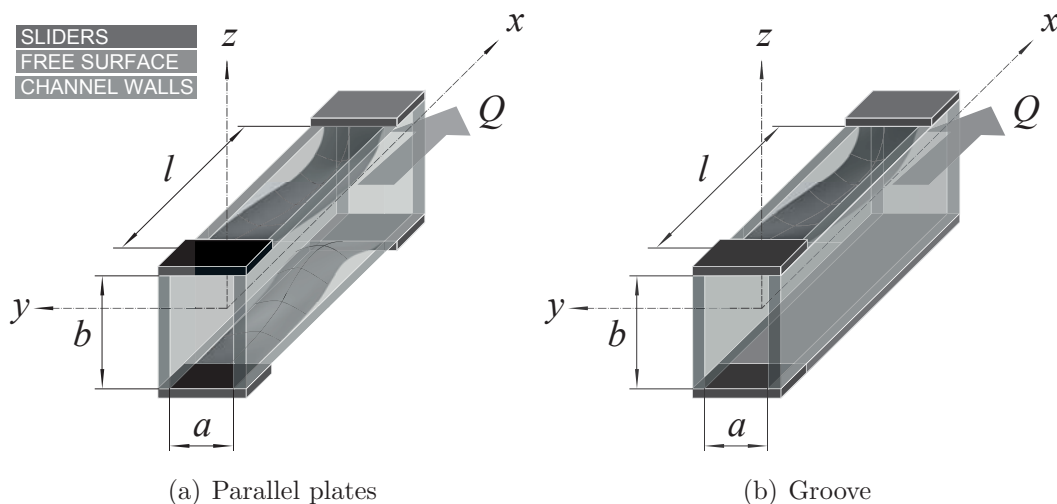


Figure 1.2: The capillary channel consisting of two glass plates (channel walls) and movable slide bars (sliders). The flow is driven along the x -axis by a pump which is located downstream of the channel. The free surfaces are pinned at the sliders edges.

The stability of the flow in said channels is the main subject of the Capillary Channel Flow (CCF) experiment. The PMD vanes shown in Figure 1.1 are simplified into capillary channels as shown in Figure 1.2. The capillary channel, investigated in this work, consists of two parallel plates. The channel's configuration can be changed with two movable sliders. Two channel configurations are considered: parallel plates (two free surfaces, Figure 1.2(a)) and groove (one free surface, Figure 1.2(b)). The capillary channel is implemented in a fluid circulation system to establish a continuous flow with variable parameters. A long time experiment was performed in the microgravity environment of the International Space Station (ISS). The test channel with the free surface(s) is observed by a High Speed High Resolution Camera (HSHRC). The images are downlinked from the ISS and evaluated by image processing. The gathered results are used to validate the mathematical model developed prior to the experiment on board the ISS.

1.1 Motivation and Background

The motivation for this work arises from a deficit in experimental and theoretical work. Only few papers are found to deal with engineering solutions for applications in surface tension tanks. A recently developed stability theory awaited the experimental validation under long term microgravity conditions. The limited test duration of previous experiments (drop tower - order of seconds, suborbital flight - order of minutes) has left many important issues unaddressed. The CCF experiment aboard the ISS provided a unique opportunity to thoroughly validate the theory and probe limits within a multidimensional parameter space.

The CCF project is an international endeavor (ZARM, NASA, DLR, PSU). It is a first long term open duct flow experiment conducted in reduced gravity environment. The main goal of the CCF experiment is to determine the shape of the free surfaces and the maximum flow rates which may be achieved in the channel without a collapse of the free surfaces. The experience gathered during the previous short-time experiments in microgravity (within the multiphase flow group at ZARM) was employed to design a new unique experimental setup. The hardware, installed on board the ISS was controllable from the ground station in Bremen. Due to the limited astronaut involvement (only hardware installation), the CCF setup had to be a “plug and play” device. The hardware development was a challenging process due to the limited resources to test the component functionality in reduced gravity environment. Drop tower experiments and suborbital flight experiments were performed prior to the ISS experiment in order to probe the functionality of the major CCF components and to perform first observations of the flow behavior in the capillary channels.

1.2 Scope of this Work

The scope of this work covers the following points:

- execution of the CCF experiment aboard the International Space Station,
- evaluation of the gathered results,
- comparison with the predictions based on the mathematical model and its verification,
- numerical modeling (1D and 3D),
- implementation of the mathematical model to study the general flow behavior in the capillary channels (which is beyond the physical constraints of the CCF experiment).

This work is structured as follows. A literature overview is given in Chapter 2, where the development of the stability theory is summarized together with the limitations of steady and unsteady flows and the previously performed short-time experiments under microgravity conditions. Chapter 3 provides an overview of the capillary channel flow models (steady and time-dependent) known from literature. Governing equations and model equations are given in both dimensional and non-dimensional form. The CCF experiment hardware is described in Chapter 4 together with the operational scenarios and the performance of the experiment. Chapter 5 provides an overview on the numerical tools employed to model the flow in capillary channels (1D, in-house developed code `ccFlow`, and 3D open source CFD code `OpenFOAM`). The results of the steady flow experiments are discussed in Chapter 6 (including the comparison with the numerical predictions). Chapter 7 provides a discussion about the general behavior of the free surfaces in the capillary channels during the steady flow, where presented findings are based on the parametric study. The results of the transient flow experiments are discussed in Chapter 8 (including the comparison with the analytic model). Chapter 9 gives an overview of the 3D simulations performed with `OpenFOAM`. In Chapter 10, the conclusions from the work are drawn.

Chapter 2

State of the Art

An open capillary channel is a structure that establishes a liquid flow path when the capillary pressure caused by the surface tension force dominates over the hydrostatic pressure induced by gravitational or residual accelerations. The cross section of the flow in the open section of the capillary channel is totally or partly confined by free surfaces. Similarities exist between the flow in the investigated open capillary channels and compressible duct flows (high-speed wind tunnels), flow in flexible tubes (arteries) or the flow in open channels (e.g. water open ducts). Each of these flows is governed by similar equations. The existence of limiting velocities is another similarity between the area-variable channel flow and compressible flows. For compressible flows, the speed of sound defines the choking velocity, whereas for the area-variable flows the limiting velocity can be defined with the speed at which waves propagate (will be discussed in Section 2.2).

In the following literature overview, both dimensional (denoted with a prime) and dimensionless quantities are presented. The scaling corresponds to the scaling of the mathematical flow model, which will be introduced in Chapter 3. The pressure $p = p'/p_c$ is scaled with the characteristic pressure $p_c = 2\sigma/a$, where a is the channel's gap distance. The velocity $v = v'/v_c$ is scaled with the characteristic velocity $v_c = \sqrt{2\sigma/(\rho a)}$. The cross-sectional area $A = A'/A_0$ is non-dimensionalized with the characteristic area $A_0 = ab$, where b is the channel's width. All lengths and the curvature h are scaled with the half of the channel's gap distance $a/2$. Complete scaling details relevant to the mathematical model considered in this work will be given in Section 3.4.

2.1 Propellant Management Devices

Propellant management devices are necessary for a spacecraft to control the position of the liquid propellant. The main function of the PMD is to keep the tank outlet to the thruster filled with fuel. The surface tension PMDs can be divided into three groups [65] (i) partial

control, (ii) total control, and (iii) total communication devices. The partial control PMDs hold a fraction of the propellant in the tank over the outlet and leave the remaining liquid free. They are generally composed of not refillable traps (closed chamber) with a porous window or refillable sponges composed of metal sheets. These devices are used in vehicles that manoeuvre considerably or use multiple engine firings. The total control surface tension PMDs hold all of the propellant over the tank outlet during all manoeuvres and are used when the slosh control is a concern. This type of device usually consists of a large compartmented container which contains almost all of the liquid when the tank is fully filled. The total communication PMDs are usually vane devices (subject of this work) designed to ensure that a flow path to the outlet is available from any position in the tank until the tank is depleted. The vanes are formed with

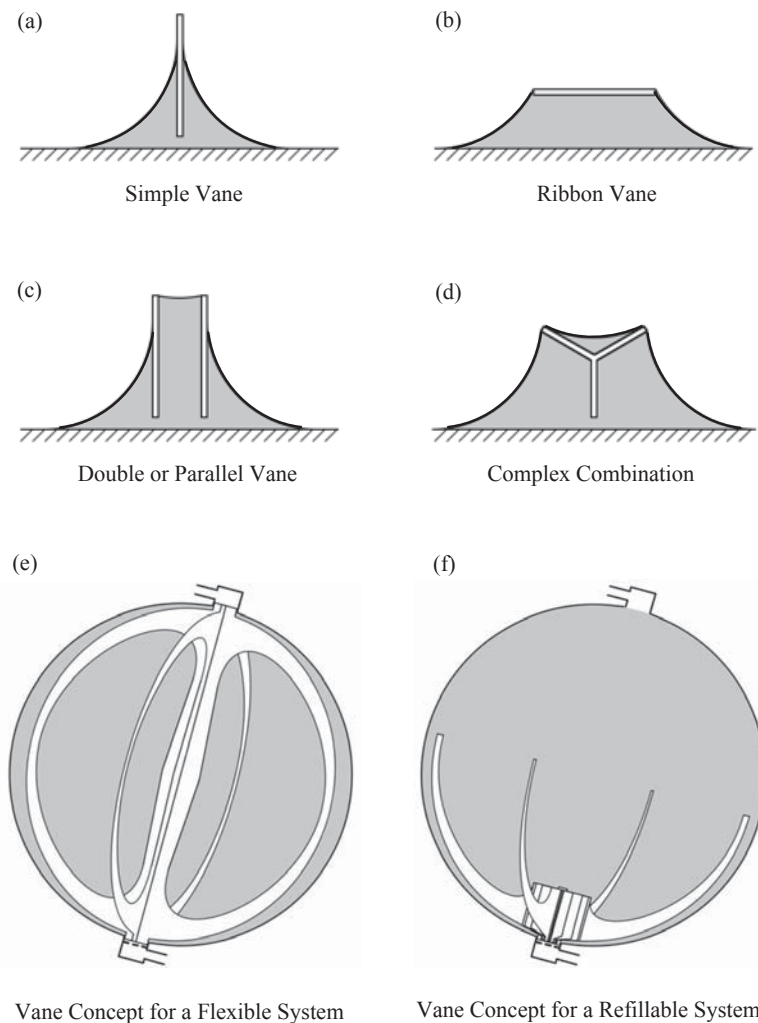


Figure 2.1: Possible vane configurations in the surface tension tank (a-d). A vane device fitted into a typical propellant tank, flexible demand system (e) and refillable system (f). Based on Jaekle [43].

metal sheets aligned along the tank’s inner walls. The simplest vanes consist of a single metal panel extending from and perpendicular to the tanks wall as shown in Figure 2.1(a).

Capillary flows along vanes are limited not only by the physical constraints of the system geometry and fluid properties, but also by spacecraft acceleration levels that can increase the BOND number¹. The flow might be interrupted due to spacecraft maneuvers causing the destabilization of the liquid-gas interface. The flow becomes unstable if either limit is exceeded. In general, to avoid gas ingestion into the flow path two technical solutions are used (depending on the specific system requirements). For low flow rates and low acceleration, the vanes are used for direct supply (Figure 2.1(e)). For much higher flow rates and higher BOND numbers, the propellant is buffered in a refillable liquid reservoir that feeds the engine during the manoeuver (Figure 2.1(f)). After the manoeuver, the reservoir is refilled by means of the vanes.

Surface tension tanks are commonly used in telecommunication satellites such as GLOBALSTAR [56] (52 satellites), INSAT [57] (24 satellites), and EUROSTAR [21] (55 satellites). An example of the OST-2 surface tension tank applied in INSAT satellites is shown in Figure 1.1.

2.2 Current State of Understanding

Surface tension devices have been used in liquid propellant tanks for almost 55 years. In spite of the broad application of PMDs there is a lack of experimental work on their flow limitations. Since the physics behind the effect of the flow rate limitation is not known, the design of vanes is based on estimations (requiring high safety factors) and the theoretical work of Jaekle [43] and Der [14]. Jaekle performed a model computation of a liquid flow through a simple T-shaped vane (metal plate positioned perpendicular to the tank wall, Figure 2.1(a)). The one-dimensional momentum equation was solved numerically, yielding the radius of curvature in the cross-sectional plane and the corresponding flow rates of steady and time-dependent flows. The solution for the free surface interface shape, however, could not be computed for all flow rates. This effect was attributed to the choking effect, without any further discussion of its physical origin. The area wave propagation velocity down a simple vane was approximated as

$$c' = \sqrt{\frac{1}{2} \frac{\sigma}{\rho R'}}, \quad (2.1)$$

where R' is the radius of curvature. Jaekle used a term “choking velocity”, assuming that c' might define an upper limit to manageable flow rates. The propagation of small disturbances traveling along the simple vanes was also studied theoretically by Der [14]. Neglecting the radius

¹The BOND number Bo measures the importance of body forces to surface tension forces. The definition of the Bo number will be given later.

of curvature in flow direction, as well as the viscosity, a linear wave equation was derived. Der postulated that the wave speed depends on the liquid volume transported in the vane. Two cases were distinguished. The wave speed depends on the fluid properties and the radius of curvature if the radius of curvature is smaller than the vane height (first case). The wave speed additionally depends on the vane height itself if the radius of curvature is larger than the vane itself (second case).

First experiments on the forced flow in open capillary channels (resembling the vanes of the PMDs) date back to 1998 and were the work of Dreyer et al. [20]. In this work the flow rate limitations in parallel plates under microgravity conditions were investigated. In the theoretical part the steady state approach given by Jaekle [43] was followed. The mathematical model was based on the one-dimensional Bernoulli equation leading to a non-linear ordinary differential equation for the radius of curvature along the free surface of the test channel. Both laminar flow and entrance pressure flow conditions were taken into account, as well as the flow conditions before the channel inlet. The experiments were based on the work of Dreyer et al. [19] who investigated the rise of liquid between parallel plates under microgravity conditions in the drop tower and showed that the velocity of the rising liquid cannot exceed a certain critical value. Further experiments with parallel plates were carried out on board the ballistic rocket TEXUS-37 (Rosendahl et al. [67, 71]). An increasing demand on the liquid during the transition (stepwise increase of the flow rate) was compensated by the liquid stored in the liquid reservoir. An inlet nozzle was applied to control the flow conditions at the channel inlet. It was shown that the capillary wave speed can be derived from the experimentally determined free surface contour. The capillary channel and the free surface were observed with a high speed camera. Both Dreyer et al. and Rosendahl et al. (drop tower and sounding rocket experiments) pointed out that very small incremental increases in flow rates are required to minimize the transient inertial effects of the flow in the capillary channels. This could be accomplished during long-term experiments within a compensated gravity environment.

An extensive experimental, numerical, and theoretical study on the flow rate limitation in the open parallel plates channel was performed by Rosendahl et al. [70], who attributed the effect of surface instability to the capillary Speed Index. The definition of the capillary Speed Index

$$S_{ca} = \frac{v}{v_{ca}} = v \sqrt{-\frac{1}{A} \frac{dA}{dh}} \quad (2.2)$$

is based on the flow velocity v and the limiting longitudinal small-amplitude wave speed v_{ca} . A is the flow cross-sectional area, and h the mean curvature. The capillary wave velocity

$$v_{ca} = \sqrt{-A \frac{dh}{dA}} \quad (2.3)$$

is the generalized wave speed of Jaekle (Equation (2.1)). Choking occurs when the capillary Speed Index reaches unity $S_{ca} = 1$ and steady flow is possible only for flow rates below this

critical value (subcritical flow). Stable, steady flow is possible in the subcritical regime and the free surface collapses at the critical point. In the one-dimensional flow model proposed by Rosendahl et al. the liquid pressure is related to the capillary pressure at the free surface including both principal radii of curvature. The model considers the convective and viscous losses, and the additional pressure loss due to the change of the velocity profile in the entrance region (entrance flow effects). For the discussion of the physical flow effects Rosendahl et al. introduced the dimensionless length \tilde{l}

$$\tilde{l} = \frac{\text{Oh}l'}{4a}, \quad (2.4)$$

where OHNESORGE number Oh relates the viscous forces to inertial and surface tension forces. The definition of the Oh number will be given later. A numerical parameter study was performed aiming on the identification of three regions in which the flow limitation is caused by either convective or frictional pressure losses, leading to distinctly different interface profiles. For flow lengths $\tilde{l} < 10^{-3}$, the frictional pressure loss vanishes and choking is caused by the convective term (momentum equation). In the transition regime ($10^{-3} \leq \tilde{l} < 10^{-1}$) both effects control the flow (convective and frictional pressure losses). For very long channels ($\tilde{l} \geq 10^{-1}$), the flow is dominated by viscous momentum transport. For $\tilde{l} \rightarrow \infty$ (pure STOKES flow), the limit of application for the choking model was shown. The analytical formulation of the critical flow rate in the purely viscous regime $\tilde{l} > 0.1$ was approximated as

$$Q_c^{an} = \frac{2}{K_{Pf}\tilde{l}}, \quad (2.5)$$

where K_{Pf} is the friction factor for the flow between parallel plates.

Srinivasan [82] studied numerically the capillary self-driven liquid flows in open parallel plates channels. He proposed a semi-analytical method for the solution of the steady three-dimensional STOKES equations. Comparing with the experimental results from Rosendahl et al. [71], the computed flow rates were approximately three times lower, which the authors attribute to the inertia in the experiment.

The stability limits of unsteady open capillary channel flow were studied by Grah et al. [32]. The steady flow model of Rosendahl et al. [70] was extended to unsteady conditions. The unsteady effect was defined by a dynamic flow rate increase during a given time period causing an additional flow rate limitation. Grah et al. postulated that the unsteady flow can be temporarily choked, remaining however stable. Thus, the theory defines three flow regimes: subcritical flow, stable supercritical flow, and unstable (supercritical) flow. The stability in the supercritical regime is explained by a pressure balance at the free liquid surface. Grah et al. introduced the Dynamic Index defined as

$$D = 1 - \frac{h^* - \chi^*}{h^* - \chi_0^*}, \quad (2.6)$$

where h^* is the capillary pressure, χ^* convective pressure at the point of the flow minimum cross-section area and χ_0^* convective pressure at the beginning of the unsteady phase. The difference $h^* - \chi^*$ tends to zero at the stability limit, thus the dynamic index reaches unity for unstable (supercritical) flow.

The existence of the numerical singularity at the critical point of the steady flow instability, postulated in previous publications, was demonstrated in detail by Grah and Dreyer [31]. The numerical singularity was attributed to the stability criterion for steady flow and represents the numerical consequence of the liquid surface collapse. Furthermore, Grah and Dreyer introduced the Equivalent Steady System (ESS) technique assuming that every unsteady state which occurs during a flow transition can be substituted by an equivalent steady state. In his method the time derivatives of the differential equation system are considered as constant at the corresponding time point. Furthermore, in the work of Grah and Dreyer the liquid surface stability model, based on the capillary pressure h^* and the flow pressure χ^* , was extended to account for the viscous pressure loss.

Convective dominated flows in open capillary channels were studied theoretically and experimentally by Rosendahl et al. [69]. Flows of this type are of particular interest since the free surfaces possesses a quasi-symmetry in the flow direction enabling the application of a new method for evaluation of the flow limits. Contrary to former approaches, this method uses an approximation of the surface curvature by means of the empirical surface profiles. Moreover, Rosendahl et al. found that the choking effect occurs independently, whether the flow limit is approached by variation of the flow rate or by the variation of the flow length.

Klatte [50] and Klatte et al.[51] studied theoretically, numerically, and experimentally the flow in capillary channels with wedge-shaped cross sections. They postulated that the capillary Speed Index is effective for the convective dominated flow, but for viscous dominated flow in the wedge, the free surface loses stability even with the Speed Index below unity. Thus, an ingestion index was proposed for viscous dominated flows.

A related phenomenon, such as capillary-driven flows in slender containers with interior edges (wedges, rounded corners, and vane gapes), were extensively investigated theoretically and experimentally. All studies are motivated by passive manipulation of the fluid interfacial flows in absence of gravitational forces. The circulation and separation of large quantities of water in spacecraft life support systems was addressed in the work of Weislogel et al. [96]. He studied experimentally (low-g flight) a passive phase separation in a urine collection system. So far, capillary solutions for water based systems aboard spacecraft were ignored due to poor and unpredictable wetting properties which control fluid configurations in capillary dominated systems. It must be noted that, without the aid of gravity, for certain processes the principal challenge is simply the one of separating two fluid phases (e.g. condensate from humid air).

Weislogel et al. [93, 95] studied the flow behavior along the interior corners of spacecraft propellant tanks after the sudden reduction of gravitational forces. The numerical results were compared with the experimental data from the drop tower (2.2 s of μg) and low-g parabolic flights. The theoretical predictions of the liquid flow were based on a nonlinear one-dimensional diffusion equation, without the strong dependence on numerical data as in the work of Ayyaswamy et al. [2] and Ransohoff et al. [63].

A broad study on the capillary-driven flow in the low-gravity environment was performed within the series of Capillary Flow Experiments (CFE) aboard the International Space Station. The CFE are designed as a collection of quantitative fundamental and applied capillary phenomena experiments conducted using handheld (by astronauts) hardware. The flow in complex geometries is studied encompassing three experimental setups, Contact Line (CFE-CL), Interior Corner Flow (CFE-ICF), and Vane Gap (CFE-VG) configuration. The first investigates the properties of the contact line which controls the interface shape, stability, and dynamics of capillary systems [45]. The second studies capillary flow in interior corners resembling the structures inside the propellant tanks [94]. The third experiment studies capillary flow when there is a gap between interior corners, such as in the gap formed by an interior vane and a tank wall of a large propellant storage tank or the near intersection of vanes in a tank with complex vane control [11, 12].

2.3 Open Channel Flow Stability Criteria

The liquid surface stability is based on the pressure interactions across the free liquid surface in the open section of the capillary channel. The flow in the capillary channel is considered as shown in Figure 2.2. The liquid is confined to the channel in the open section by capillary forces only. The curvature of the free surface balances the pressure differences across the interface. The capillary pressure, defined with the YOUNG-LAPLACE Equation $h^* = R_1^{*-1} + R_2^{*-1}$, has to compensate two flow-induced pressure flow effects. Firstly, the convective pressure χ^* caused by the convective acceleration vdv/dx . Secondly, an additional pressure effect, which is the difference $h^* - \chi^*$ caused by the the local acceleration dv/dt of an unsteady flow. In general, the capillary pressure (surface tension) enhances the stability of the free surface, whereas the convective pressure and the effect of the local acceleration act contrarily. In the following, two criteria for the surface stability will be formulated of which at least one has to be fulfilled to assure the stability. The pressure balance at the point of the minimum cross-section x^* as shown in Figure 2.2 can be defined as [32]

$$\int_0^{x^*} \frac{dv}{dt} dx = h^* - \chi^* . \quad (2.7)$$

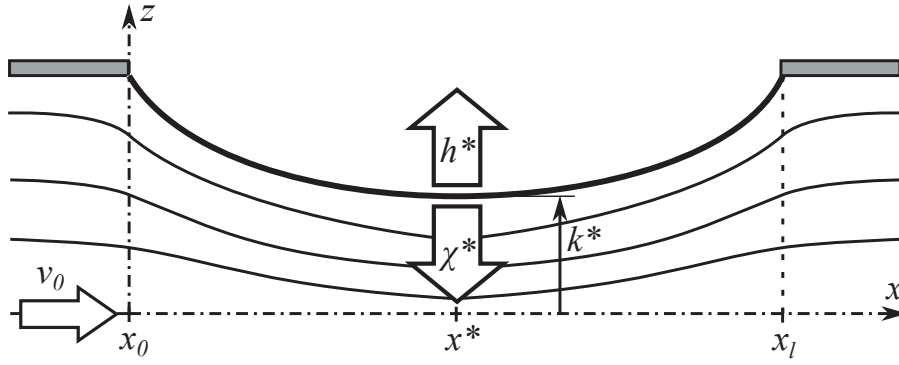


Figure 2.2: Steady equilibrium of the capillary pressure h^* and the convective pressure χ^* .

The irreversible pressure loss effects are neglected and the convective pressure (square function of the velocity) increases significantly at the channels throat. Hence, the convective pressure has a high potential for destabilization and plays a significant role in the liquid stability.

2.3.1 Flow Rate Limitation of Steady Flow

For steady flow, the pressure balance (2.7) at the channel position x^* simplifies to

$$h^* = \chi^* . \quad (2.8)$$

Figure 2.3(a) shows a generic steady pressure diagram at the point of the minimum cross section. The thin χ_Q^* lines represent the theoretical behavior of the convective pressure χ^* over the contour height k^* for a constant flow rate $Q = v^* A^*$. The bold line shows the capillary pressure h^* , which is the function of the curvature of the free surface. In general, with decreasing contour height k^* at the point $x = x^*$, the curvature of the free surface increases causing an increase of the capillary pressure h^* . A steady state can be defined at the intersection of the h^* and χ_Q^* lines, for a given flow rate Q (e.g., point **a** in Figure 2.3(a)). Qualitative comparison of the pressure curves in Figure 2.3(a) shows a higher gradient of the h^* line compared to the χ_Q^* lines. Even a small change of k^* caused by the free surface movements (due to external perturbations, e.g. change of boundary conditions) leads to a change of the capillary pressure along the h^* line and of the convective pressure along the χ_Q^* line (constant Q is assumed). Since the h^* line is steeper than the χ_Q^* line, the capillary pressure always acts in a stabilizing way and compensates the convective pressure. Hence, the stability criterion for steady flow can be formulated based on the gradients as

$$\left| \frac{dh^*}{dk^*} \right| > \left| \frac{d\chi^*}{dk^*} \right| . \quad (2.9)$$

With increasing flow rate, the point **a** in Figure 2.3(a) moves upwards along the h^* line (the free surface bends inwards, and the capillary pressure increases). The gradient of the h^* line decreases slightly and the gradient of the χ_Q^* line increases significantly for smaller k^* values.

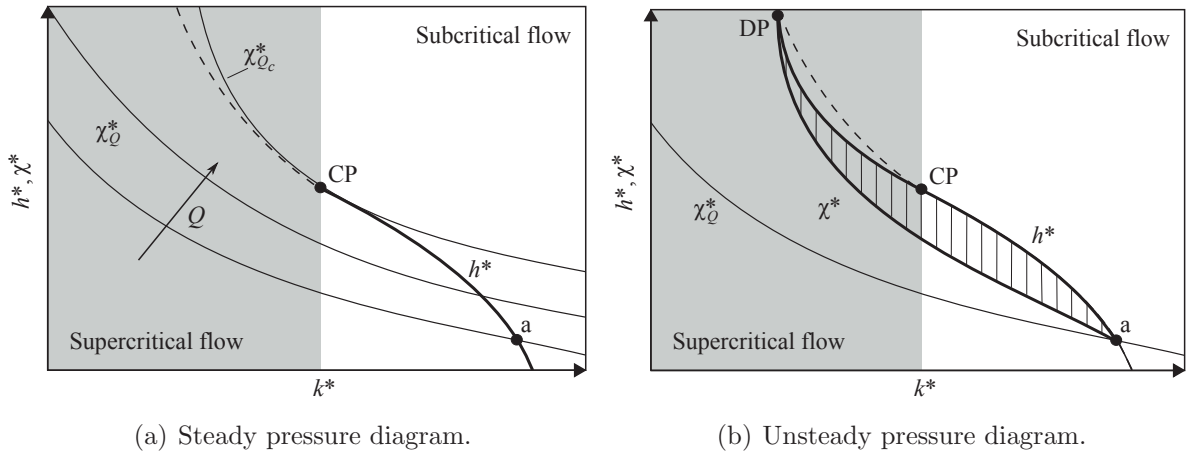


Figure 2.3: Pressure diagrams at the point $x = x^*$, where h^* is the capillary pressure, χ^* is the theoretical value of the convective pressure, and k^* is the free surface contour. The critical point CP defines the limit of the steady flow. For unsteady flow (b) the liquid surface collapse occurs at the destabilization point DP.

Consequently, the difference of the gradients in Equation (2.9) decreases. The gradients are equal when the critical point CP is reached, and the corresponding flow rate defines the critical rate (limit of the stable flow). The dashed line in Figure 2.3(a) represents the theoretical supercritical solution of no practical meaning for the steady flow theory. It will be shown later that it corresponds to the stability limit of unsteady flow.

Furthermore, rearranging inequality (2.9) and combining it with the small amplitude wave speed (2.3) yields the capillary Speed Index at the point of the minimum cross section

$$S_{ca} = \frac{v^*}{v_{ca}^*} = v^* \sqrt{-\frac{1}{A^*} \frac{dA^*}{dh^*}}, \quad (2.10)$$

which bears similarities to Rosendahl et al. definition (2.2). The dependency of the S_{ca} on the flow rate is shown in Figure 2.4. At the critical point CP the velocities are equal $v_{ca}^* = v^*$, and the Speed Index reaches unity, $S_{ca} = 1$. Any disturbance traveling upstream at the speed of sound, e.g. an infinitesimal increase of the flow rate (pump located downstream from the channel outlet) cannot pass the minimum cross-section point $x = x^*$. In such case, the flow rate at the inlet remains unchanged. To satisfy continuity, surrounding gas has to be ingested into the channel. Thus, the free surface collapses and gas ingestion occurs. This phenomenon (choking) bears similarities to compressible duct flows e.g., flow in a DE LAVAL nozzle or an orifice. Here, the limiting velocity is the speed of sound, and the MACH number approaches unity at the critical point.

The effect described above might be denoted as a “wave speed limitation” with the limiting mechanism of choking. For sufficiently long channels ($\tilde{l} > 0.1$), an effect of “viscous limitation” causes the flow rate limitation, as shown by Rosendahl et al. [69].

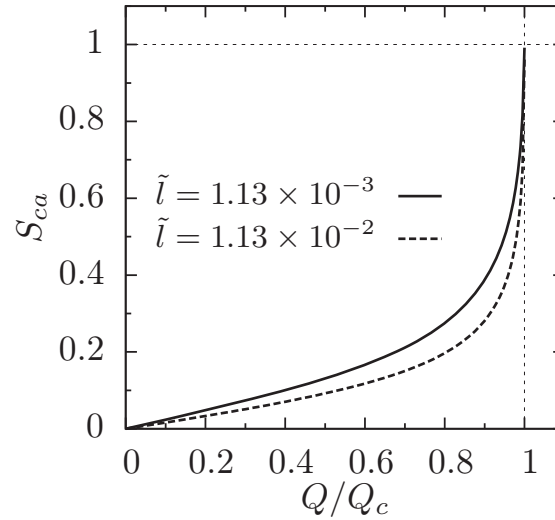


Figure 2.4: Numerically predicted Speed Index S_{ca} as a function of the flow rate Q for the parallel plates. Two flow lengths \tilde{l} are chosen for comparison. The mathematical flow model (will be discussed in Section 3.4) is solved with finite differences (will be discussed in Section 5.1).

2.3.2 Flow Rate Limitation of Unsteady Flow

For unsteady flow, the acceleration pressure effect is taken into account. The capillary pressure h^* and the convective pressure χ_Q^* are not equal during the flow rate transition. Figure 2.3(b) shows a generic unsteady pressure diagram at the point of the minimum cross section. The point **a** (subcritical steady state) depicts the beginning of the unsteady phase. During the transition the free surface is drawn into the channel and the contour height k^* decreases. Consequently, the capillary pressure h^* moves along the bold line of the pressure diagram. The difference $h^* - \chi^*$ (marked with hatched lines in Figure 2.3(b)) represents the dynamic pressure effect, caused by the acceleration term in Equation (2.7). Owing to the unsteady terms no singularity occurs for the numerical solution at the critical point CP [32]. The flow remains stable and the supercritical flow regime on the left-hand side of the critical point CP can be reached in the case of dynamic flow. The Speed Index (2.10) is a function of the flow cross-sectional area A^* and the curvature h^* only and can be applied to the unsteady case as well. As for steady flow it reaches the value of $S_{ca} = 1$ at the CP in Figure 2.3(b). In the supercritical regime, the communication between the channel outlet and inlet is interrupted. Increasing flow rate demand on the outlet is not followed by the inlet flow rate. The imbalance between the outlet and inlet flow rate is compensated by liquid displacement. The difference $h^* - \chi^*$ decreases for decreasing k^* in the supercritical regime. In the supercritical regime the free surface is further drawn into the channel. This leads to an increase of the local curvature and a significant

increase of the h^* -line gradient. When the convective pressure χ^* reaches the value of the capillary pressure h^* , the free liquid surface collapses (the destabilization point DP in Figure 2.3(b)). Hence, the supercritical unsteady stability limit criterion can be formulated as

$$h^* < \chi^* . \quad (2.11)$$

According to definition of the Dynamic Index given in Equation 2.6, χ_0^* is the convective pressure at the beginning of the unsteady phase. This corresponds with point **a** in Figure 2.3(b)). The difference $h^* - \chi^*$ tends to zero at the stability limit, thus an unsteady open capillary channel flow is stable if the Dynamic Index does not reach the value $D = 1$ in the supercritical area.

2.4 Limitation of Ground Based Experiments

Terrestrial experiments are limited by the hydrostatic pressure acting on the free liquid surfaces. Consequently, the OHNESORGE number is limited. Considering a horizontal flow between parallel plates (Figure 1.2(a)), the limits can be estimated with the following relation

$$\rho g_z a \approx \frac{2\sigma}{a} , \quad (2.12)$$

where the term on the left-hand side is the maximal hydrostatic pressure in the channel of gap distance a . The term on the right hand side represents the differential (capillary) pressure across the liquid interfaces. It is derived from the YOUNG-LAPLACE equation $p' - p'_a = -\sigma(R'^{-1} + R'^{-1})$, where the radius of curvature in flow direction x' is neglected ($R'_1 = -a/2, R'_2 \rightarrow \infty$). The ratio between the gravity and surface tension forces can be expressed with the BOND number defined as $Bo_z = \rho g_z ab / 2\sigma$, where $g_z = 9.8 \text{ m/s}^2$ is the gravitational acceleration on Earth. The maximal gap distance in a ground based experiment and the minimal OHNESORGE number can be estimated as

$$a_{max} = \sqrt{\frac{2Bo_z\sigma}{\rho g_z}} , \quad Oh_{min} = \frac{\mu}{\sqrt{2a_{max}\rho\sigma}} . \quad (2.13)$$

Since the stability limit in considered channels is not known, $Bo_z < 0.01$ is required. For the standard test liquids, the obtained limitations are shown in Table 2.1. For the test liquid HFE-7500 used in the CCF experiment, the maximal gap distance is $a_{max} = 0.1 \text{ mm}$, and the minimal Oh number $Oh = 12.5 \times 10^{-3}$. The range to be investigated aboard the International Space Station is however $5 \times 10^{-3} > Oh > 5 \times 10^{-4}$. Large Oh number lead to a viscous dominated flow behavior and convective as well as inertia related effects cannot be studied.